Supporting information

A Compact Planar Low-Energy-Gap Molecule with Donor–Acceptor–Donor Nature Based on a Bimetallic Dithiolene Complex

Mikihiro Hayashi,[*,†] Kazuya Otsubo,[†] Tatsuhisa Kato,[□] Kunihisa Sugimoto,[§] Akihiko Fujiwara[#] and Hiroshi Kitagawa[*,†,‡]

[†]*Division of Chemistry, Graduate School of Science, Kyoto University, Kitashirakawa Oiwake-cho, Sakyo-ku, Kyoto 606-8502, Japan*

[§]*Japan Synchrotron Radiation Research Institute (JASRI), SPring-8, 1-1-1 Kouto, Sayo-cho, Sayo-gun, Hyogo 679-5198, Japan*

[□]*Institute for the Promotion of Excellence in Higher Education, Kyoto University, Yoshida-Nihonmatsu, Sakyo-ku, Kyoto 606-8501, Japan*

[#]*Department of Nanotechnology for Sustainable Energy, Graduate School of Science and Technology, Kwansei Gakuin University, Gakuen, Sanda, Hyogo 669-1337, Japan*

[‡]*Core Research for Evolutional Science and Technology (CREST), Japan Science and Technology Agency (JST), 7 Goban-cho, Chiyoda-ku, Tokyo 102-0075, Japan*

Contents

1. Experimental details.

1.1 Materials.

2,3-pyradine-4,5-dithiolate was prepared according to the previous report(1). In a synthesis, 1,3,4,6-tetrathiapentalene-2,5-dione (TPD) (Tokyo Chemical Industry Co., Ltd.), sodium (Kishida Chemical Co., Ltd.), nickel(II)chloride,6-hydrate ($NiCl\cdot6H_2O$) (Wako Pure Chemical Industries, Ltd.), sodium hydroxide (NaOH) (Wako Pure Chemical Industries, Ltd.) and tetrabutylammonium bromide (TBABr) (Wako Pure Chemical Industries, Ltd.) were used without any purification. Water was purified by ion exchange culoums. Methanol, dimethylsulphoxide (DMSO) and diethylether at commercially available grade were used. In a NMR measurement, DMSO-d6 (Wako Pure Chemical Industries, Ltd.) was used. In an electrochemical measurement, tetrabutylammonium perchlorate ($TBAClO_4$) (special prepared regent) (Nacalai Tesque, Inc.), ferrocene (Wako Pure Chemical Industries, Ltd.) and DMSO (infinity Pure grade) (Wako Pure Chemical Industries, Ltd.) were adopted. In a chemically reduced reaction, cobaltocene ($CoCp_2$) (Sigma-Aldrich Co. LLC.) and DMSO (for spectrochemical analysis) (Wako Pure Chemical Industries, Ltd.) were used. In an absorption measurement, DMSO (for spectrochemical analysis) (Wako Pure Chemical Industries, Ltd.) and KBr (crystal block) (Wako Pure Chemical Industries, Ltd.) were utilized as diluting agents.

1.2 Synthesis.

Tetrabutylammonium(μ-tetrathiooxarate)bis[(2,3-pyradine-4,5-dithiolato)nickelate(II)];
TBA_2[(**tto**){Ni(pdt)}$_2$] (complex **1)**

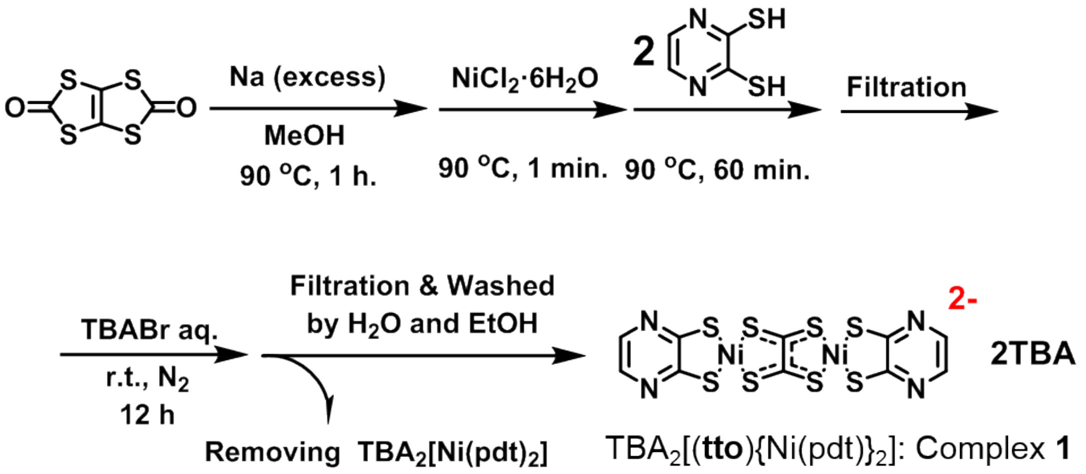

Under an ambient temperature and an inert atmosphere, 1,3,4,6-tetrathiapentalene-2,5-dione (5.19 g, 25 mmol) was dissolved into a solution of excess amount of sodium in methanol (200 mL). The mixture was stirred at 90^{o}C for 1 hour. During this reaction, the color of solution was changed from light yellow to dark brown. Then, $NiCl{\cdot}6H_2O$ (7.58 g, 32 mmol) in methanol (100 mL) and 2,3-pyradine-4,5-dithiolate (7.15 g, 50 mmol) in basic aqueous solution (100 mL) were added to this reaction mixture in this order. After this solution had been stirred for 1 hour at 90^{o}C, an unresolved solid was filtered and tetrabutyammonium bromide (20 g, 62 mmol) in water (100 mL) was added to the filtrate. After this filtered solution had been stirred for 6 hours at ambient temperature, an unresolved solid was generated. By filtration, this solid and filtrate were separated. By evaporating this filtrate, bis(2,3-pyradine-4,5-dithiolato)nickelate(II) ($TBA_2[Ni(pdt)_2]$) was obtained as an orange powder and its single crystal was grown by diffusing gas of diethyether into its acetone solution (7.9 g, 9.6 mmol, 30%). On the other hand, the above mentioned solid was dissolved in acetone, and reside was filtered again. After evaporating acetone from this filtrate, dark brown powder (TBA_2[(**tto**){Ni(pdt)}$_2$]: complex **1**) was obtained. This residue was recrystallized from DMSO and diethylether to afford rod shaped black crystal (1.2 g, 1.1 mmol, 3.4%). All experiments were performed by use these crystalline samples.

TBA_2[(**tto**){Ni(pdt)}$_2$] (complex **1**)

^{1}H NMR (DMSO-d6, 600 MHz): δ = 7.86 (4H, s), 3.15 (16H, m), 1.55 (16H, m), 1.30 (16H, m), 0.92 (24H, t, *J* = 6.4 Hz). Anal. Calcd for $C_{42}H_{76}N_6Ni_2S_8 \cdot$ 2DMSO: C, 73.70; H, 4.92; N, 3.57. Found: C, 73.98; H, 5.09; N, 3.53.

TBA$_2$[Ni(pdt)$_2$]

^{1}H NMR (DMSO-d6, 600 MHz): δ = 7.31 (4H, s), 3.18 (16H, m), 1.57 (16H, m), 1.30 (16H, m), 0.91 (24H, t, *J* = 6.4 Hz). Anal. Calcd for $C_{40}H_{76}N_6NiS_4$: C, 58.02; H, 9.25; N, 10.15. Found: C, 57.79; H, 9.27; N, 10.15.

1.3. ^{1}H NMR spectra.

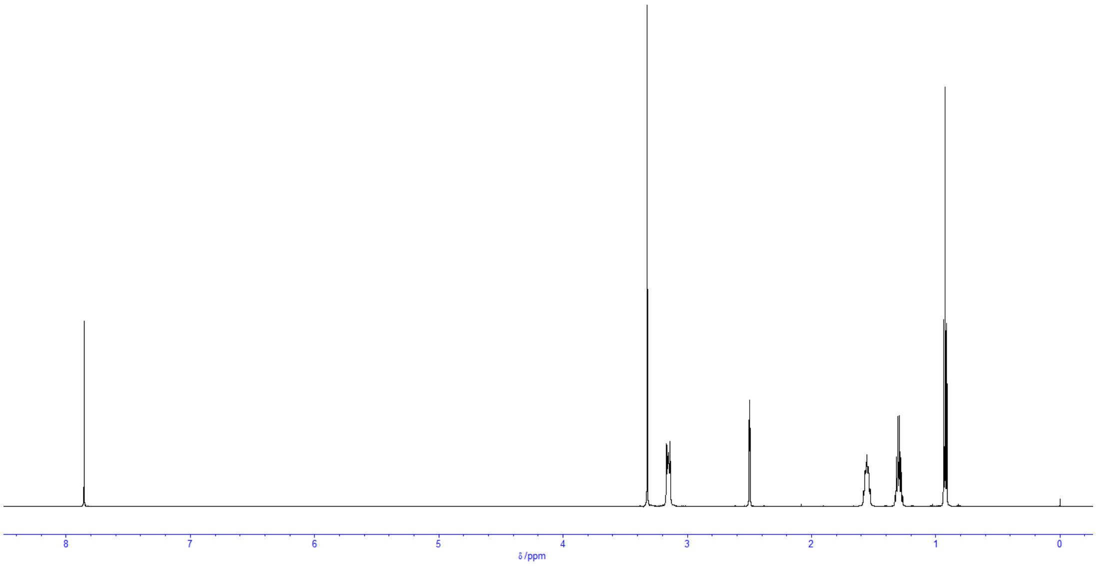

Fig. S1a. ^{1}H-NMR spectrum of complex **1** in DMSO-d^6.

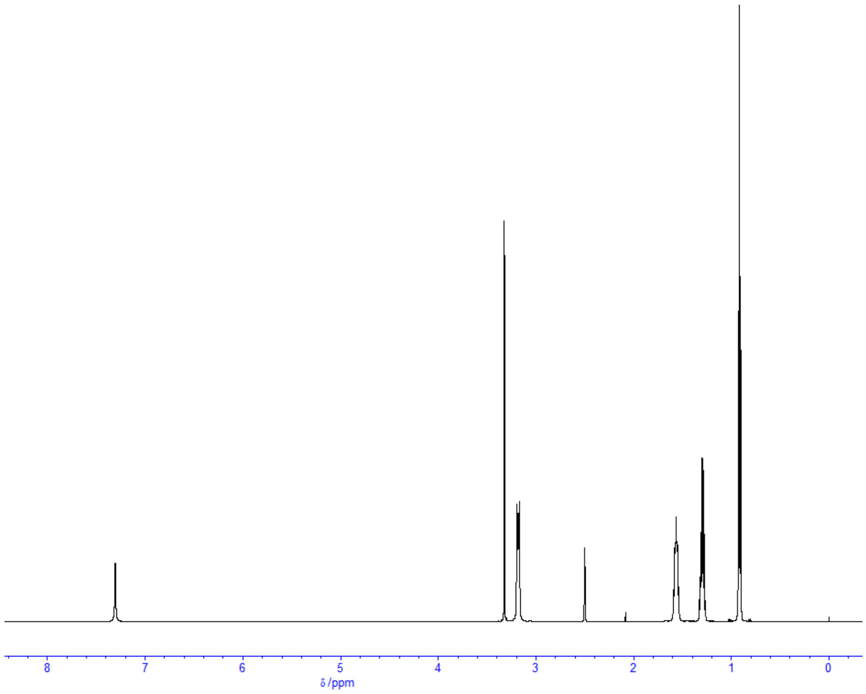

Fig. S1b. ^{1}H-NMR spectrum of $Ni(pdt)_2TBA_2$ in DMSO-d^6.

1.4. X-ray single crystal structural analysis.

For structural analysis, the diffraction data of single crystal of complex **1** under various temperatures were collected by use of the synchrotron X-ray at the BL02B1 beam-line in SPring-8 with a Rigaku Mercury2CCD detector. In addition, the diffraction data of single crystal of $TBA_2[Ni(pdt)_2]$ at 100 K was collected by use of a Bruker SMART APEX II CCD (charge-coupled device) area detector and a Rigaku AFC-7R Mercury CCD area detector with graphite–monochromated Mo *K*α radiation. Empirical absorption corrections using equivalent reflections and Lorentzian polarization correction were performed using the program Crystal Clear 4.0. The structures were refined against F^2 using SHELXL-97.

1.5. DFT calculation.

The three-parameterized Becke-Lee-Yang-Parr (B3LYP) hybrid exchange-correlation function was employed. As a basis set, 6-31+G (d, p) (C, H, N, S) and Lanl2dz (Ni) were used for $[(\mathbf{tto})\{Ni(pdt)\}_2]^{2-}$ and $[Ni(pdt)_2]^{2-}$, on the other hand, 6-31G was used for tto^{2-}. The geometries were optimized with symmetry constraints. TD-DFT calculation was executed under the same condition. Solvent effects were not considered in any of the processes.

These calculations were implemented with the Gaussian 09W program.

1.6. Electrochemical measurement.

A series of measurements was carried out in a standard one-component cell, using 3mmϕ glassy carbon (BAS Inc.) as a working electrode, platinum wire (BAS Inc.) as a counter electrode, and Ag/$AgClO_4$ reference electrode (0.01M $AgClO_4$ in 0.1M-TBAP/acetonitrile, house–made). As a supporting electrolyte tetrabutylammonium perchlorate was used. As an internal standard, ferrocene was added after each measurement. Electrochemical data were acquired with an ALS 650B voltammetric analyzer (BAS).

1.7. Electrolytic absorption measurement.

In this measurement, a house–made quartz cell with three–electrode system (3mmϕ glassy carbon (BAS Inc.) as a working electrode, platinum mesh (home–made) as a counter electrode, and Ag/$AgClO_4$ reference electrode (0.01M $AgClO_4$ in 0.1M-TBAP/acetonitrile, house–made)) was used. As a supporting electrolyte tetrabutylammonium perchlorate was used.

1.8. Measurement of Electron spin resonance.

Electron spin resonance (ESR) spectra of complex **1** and complex **1** with one equivalent of $CoCp_2$ were measured in frozen DMSO at 8 K. All samples were prepared and measured in an inert condition.

1.9. Apparatus.

NMR study were performed by JEOL spectrometer (600MHz). Absorption spectra were measured with Jasco V-570 UV/Vis spectrometers. Resonant Raman spectra were collected by Jasco NRS-1000 and He-Ne laser (λ = 632 nm) was used for excitation light source. Electrochemical data were acquired with BAS ALS 650B voltammetric analyzer. ESR spectroscopy was recorded by using Bruker EMX, and cryostat ESR 900 of Oxford instrument was utilized for continuous He supply.

2. Variable temperature resonance Raman spectroscopic measurement.

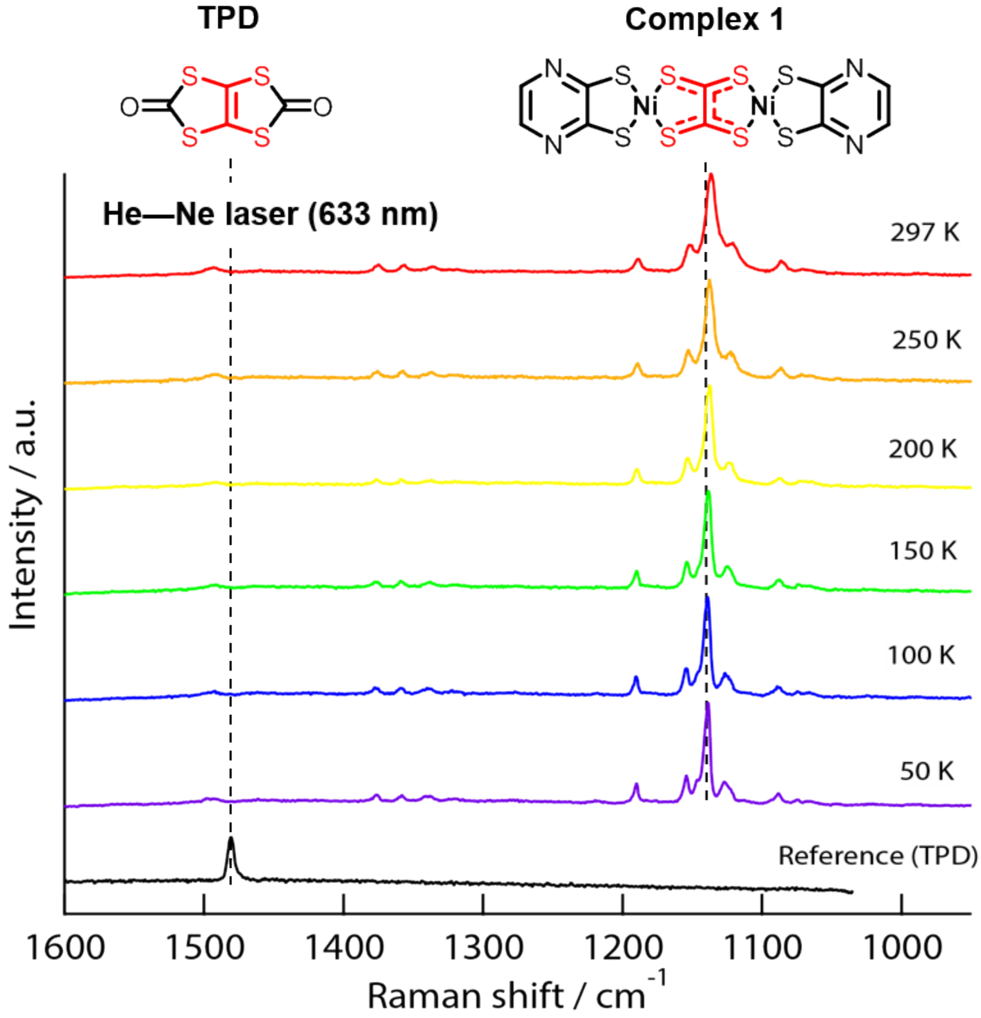

Fig. S2. Resnance Raman spectra of complex **1** from 50 to 297 K. The compared resonance of C-C was observed around 1480 cm^{-1} by use of 1,3,4,6-tetrathiapentalene-2,5-dione (TPD).

3. Temperature dependency of molecular geometry.

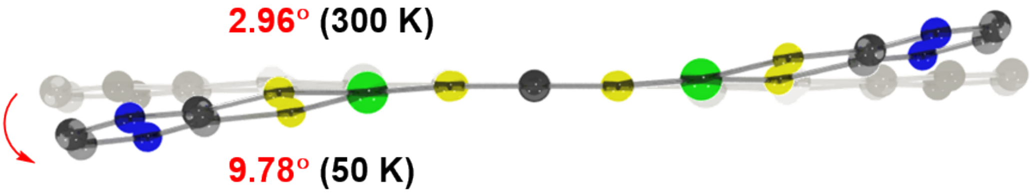

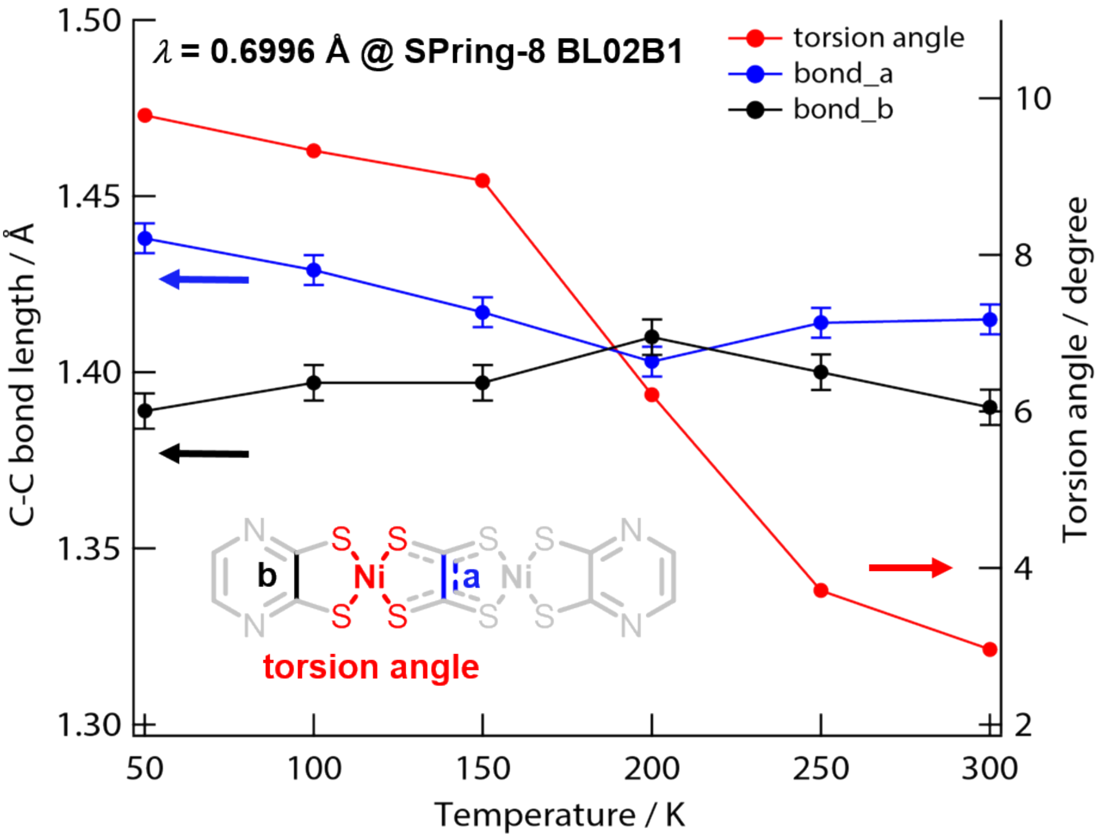

Fig. S3. Temperature dependency of molecular torsion and bond length.

Table S1 Data quality of single crystal X-ray diffraction measurement at SPring-8.

temperature / K	bond length / Å		angle / degree	obtained parameter	
	a	b	torsion	R	GOF
300	1.415(8)	1.39(10)	2.96	0.0755	0.840
250	1.416(9)	1.40(10)	3.71	0.0901	0.920
200	1.397(9)	1.41(10)	6.02	0.0902	0.976
150	1.417(9)	1.397(9)	8.95	0.0911	1.028
100	1.429(8)	1.397(9)	9.33	0.0878	1.057

(a) Crystal data of complex **1** @ 50 K: $C_{46}N_6Ni_2O_2S_{10}$; formula weight = 1106.55, monoclinic, $P2_1/n$, a = 10.877(3) Å, b = 19.073(5) Å, c = 13.930(4) Å, β = 94.607(7)°, V = 2880.4(13) Å^3, Z = 2, D_c = 1.276 g cm^{-3}, No. of reflections measured = 18,425 (No. of unique reflections = 6536), R_1 ($I > 2.00\sigma(I)$) = 0.0866, wR_2 = 0.2407 (all data), GOF = 1.079.

(b) Crystal data of complex **1** @ 100 K: $C_{46}N_6Ni_2O_2S_{10}$; formula weight = 1106.55, monoclinic, $P2_1/n$, a = 10.895(3) Å, b = 19.189(5) Å, c = 13.957(4) Å, β = 94.674(7)°, V = 2908.3(13) Å^3, Z = 2, D_c = 1.264 g cm^{-3}, No. of reflections measured = 18,421 (No. of unique reflections = 6,562), R_1 ($I > 2.00\sigma(I)$) = 0.0878, wR_2 = 0.2485 (all data), GOF = 1.057.

(c) Crystal data of complex **1** @ 150 K: $C_{46}N_6Ni_2O_2S_{10}$; formula weight = 1106.55, monoclinic, $P2_1/n$, a = 10.885(4) Å, b = 19.278(6) Å, c = 13.961(5) Å, β = 94.810(7)°, V = 2919.1(17) Å^3, Z = 2, D_c = 1.287 g cm^{-3}, No. of reflections measured = 18,395 (No. of unique reflections = 6,572), R_1 ($I > 2.00\sigma(I)$) = 0.0911, wR_2 = 0.2719 (all data), GOF = 1.028.

(d) Crystal data of complex **1** @ 200 K: $C_{46}N_6Ni_2O_2S_{10}$; formula weight = 1106.55, monoclinic, $P2_1/n$, a = 10.7705(17) Å, b = 19.924(3) Å, c = 13.848(2) Å, β = 96.499(7)°, V = 2952.6(8) Å^3, Z = 2, D_c = 1.245 g cm^{-3}, No. of reflections measured = 19,126 (No. of unique reflections = 6,721), R_1 ($I > 2.00\sigma(I)$) = 0.0902, wR_2 = 0.2933 (all data), GOF = 0.976.

(e) Crystal data of complex **1** @ 250 K: $C_{46}N_6Ni_2O_2S_{10}$; formula weight = 1106.55, monoclinic, $P2_1/n$, a = 10.7047(15) Å, b = 20.555(3) Å, c = 13.8324(19) Å, β = 98.106(7)°, V = 3013.2(7) Å^3, Z = 2, D_c = 1.219 g cm^{-3}, No. of reflections measured = 19,540 (No. of unique reflections = 6,859), R_1 ($I > 2.00\sigma(I)$) = 0.0901, wR_2 = 0.2863 (all data), GOF = 0.920.

(f) Crystal data of complex **1** @ 300 K: $C_{46}N_6Ni_2O_2S_{10}$; formula weight = 1106.55, monoclinic, $P2_1/n$, a = 10.6962(14) Å, b = 20.721(3) Å, c = 13.8764(19) Å, β = 98.222(7)°, V = 3044.0(7) Å^3, Z = 2, D_c = 1.207 g cm^{-3}, No. of reflections measured = 19,774 (No. of unique reflections = 6924), R_1 ($I > 2.00\sigma(I)$) = 0.0755, wR_2 = 0.2428 (all data), GOF = 0.840.

These crystal structures of complex 1 at various temperatures (50, 100, 150, 200, 250 and 300 K) have been deposited at The Cambridge Crystallographic Data Center as publication numbers CCDC 1063807, 1063808, 1063809, 1063810, 1063811 and 1063812.

4. Thermal stability.

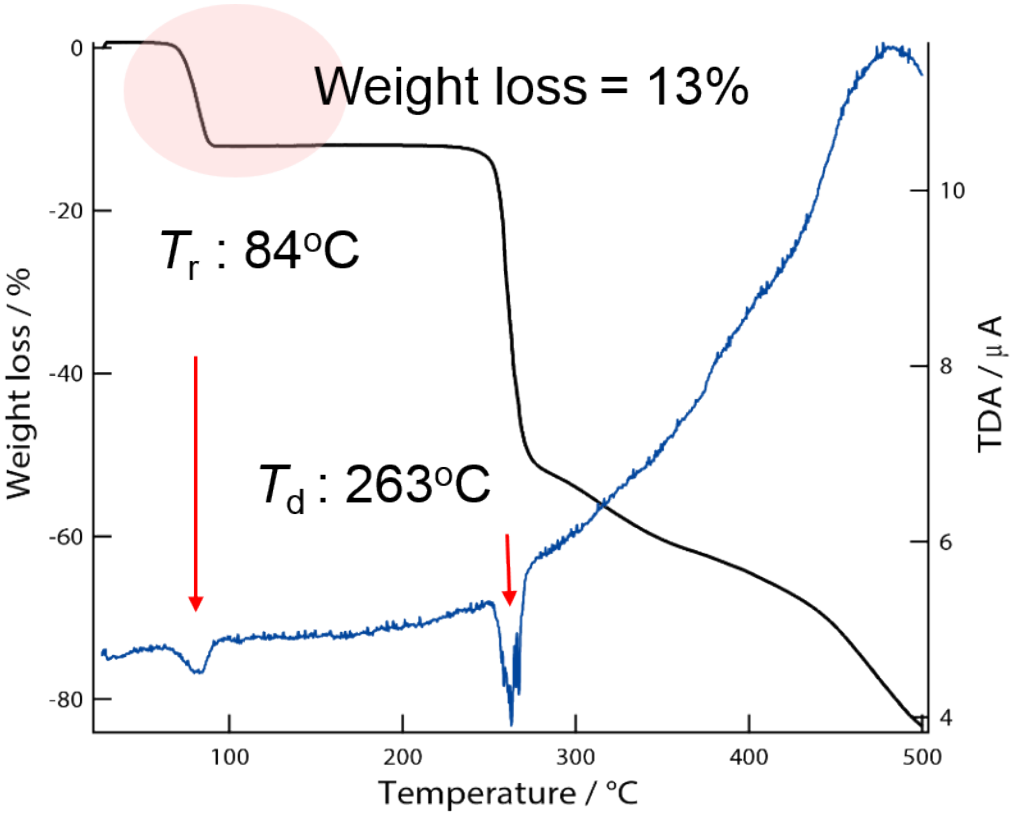

Fig. S4. TG analysis of complex **1**. Desorption temperature (***T***$_r$) of DMSO molecule and Decomposition temperature (***T***$_d$) of complex **1** were graphically illustrated. The weight loss of 13% confirmed to the calculated value of DMSO molecule from the result of elemental analysis.

5. The result of DFT calculation.

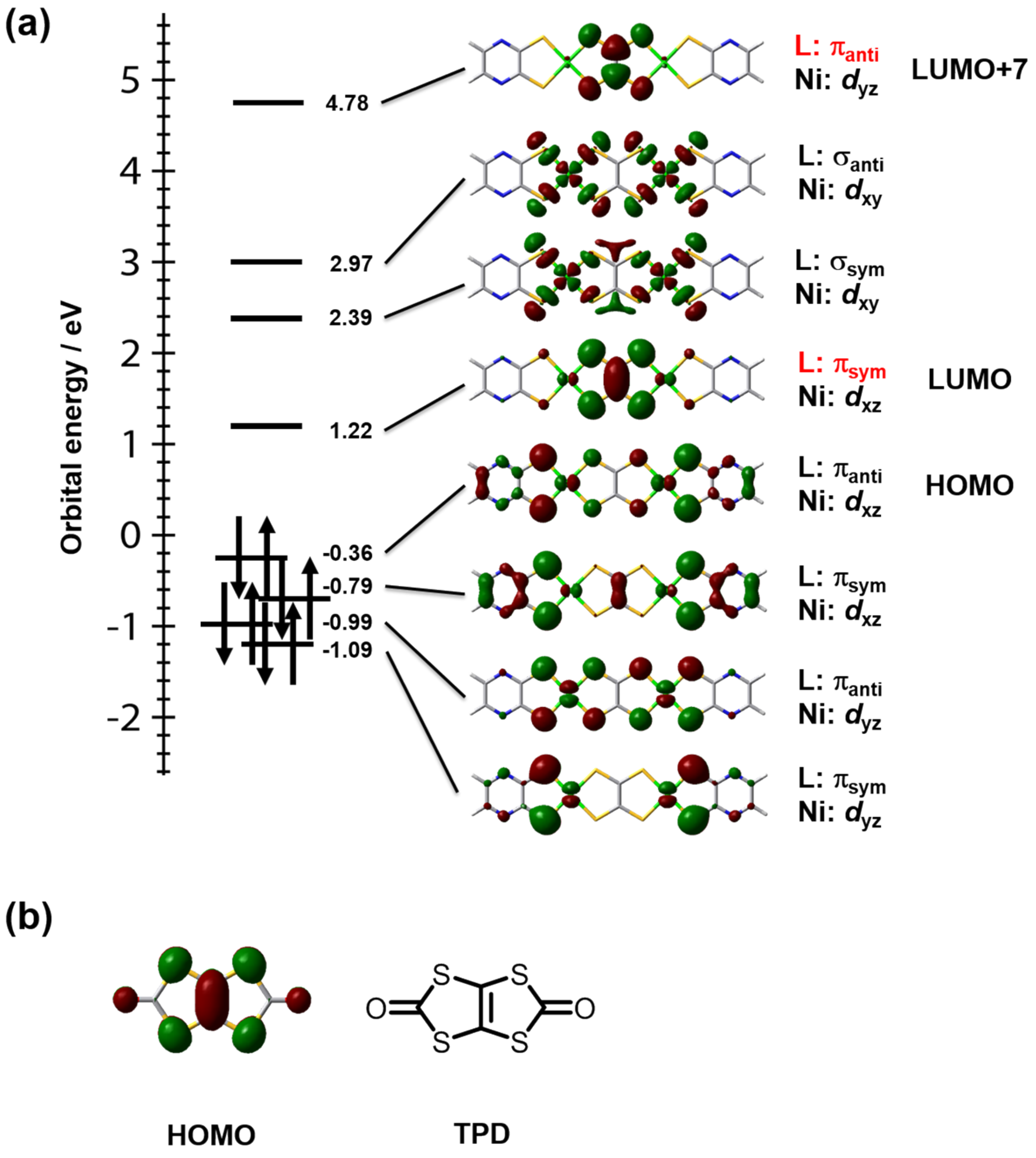

Fig. S5. (a)The result of DFT calculation of complex **1**. (b)Calculated HOMO of TPD

The calculation of single point energy of complex **1** with consideration of a solvation effect by DMSO was performed by use of Gaussian 09 with SCRF (PCM,Solvent=DMSO) method. As a result, more reduced energy (0.74 eV) was obtained. This underestimation has often been observed in the result of DFT calculation. This result makes sense because it clearly explains that solvation interaction gives the difference between observed and calculated HOMO–LUMO gap. The result of SCRF calculation was attached as follows.

```
**********************************************************************
Population analysis using the SCF density.
**********************************************************************

Orbital symmetries:
Occupied   (AU) (AG) (AG) (AU) (AG) (AU) (AU) (AG) (AU) (AG)
(AG) (AU) (AU) (AG) (AU) (AG) (AG) (AU) (AG) (AU)
(AG) (AU) (AU) (AG) (AG) (AU) (AU) (AG) (AG) (AU)
(AG) (AU) (AG) (AU) (AU) (AG) (AG) (AU) (AG) (AU)
(AG) (AU) (AG) (AU) (AG) (AU) (AU) (AG) (AG) (AU)
(AG) (AU) (AU) (AG) (AU) (AG) (AG) (AU) (AG) (AU)
(AG) (AU) (AG) (AU) (AG) (AU) (AG) (AU) (AU) (AG)
(AU) (AG) (AU) (AG) (AU) (AG) (AG) (AU) (AG) (AU)
(AG) (AU) (AU) (AG) (AU) (AG) (AU) (AG) (AG) (AU)
(AG) (AU) (AG) (AU) (AU) (AG) (AG) (AU) (AG) (AG)
(AU) (AU) (AG) (AU) (AG) (AU) (AU) (AG) (AG) (AU)
(AU) (AG) (AU) (AG) (AG) (AU) (AU) (AG) (AU) (AG)
(AG) (AU) (AG) (AG) (AU) (AG) (AU) (AU) (AG) (AG)
(AU) (AU) (AG) (AG) (AU) (AU) (AG) (AU) (AG)
Virtual    (AG) (AU) (AU) (AG) (AU) (AU) (AG) (AU) (AG) (AU)
(AG) (AU) (AG) (AG) (AU) (AU) (AU) (AG) (AG) (AG)
(AU) (AG) (AU) (AU) (AU) (AG) (AG) (AG) (AU) (AG)
(AU) (AG) (AU) (AG) (AU) (AG) (AU) (AG) (AU) (AG)
(AG) (AU) (AU) (AU) (AG) (AU) (AG) (AU) (AG) (AG)
(AU) (AG) (AG) (AU) (AG) (AU) (AU) (AU) (AU) (AG)
(AG) (AU) (AG) (AU) (AU) (AG) (AG) (AG) (AG) (AU)
(AU) (AU) (AG) (AG) (AU) (AG) (AU) (AU) (AG) (AG)
(AU) (AU) (AU) (AG) (AU) (AG) (AU) (AG) (AU) (AG)
(AG) (AU) (AU) (AG) (AG) (AG) (AU) (AG) (AU) (AU)
```

```
(AG) (AG) (AU) (AG) (AU) (AU) (AU) (AG) (AG) (AU)
(AG) (AU) (AG) (AU) (AU) (AG) (AU) (AG) (AG) (AU)
(AG) (AU) (AG) (AU) (AU) (AG) (AG) (AU) (AG) (AU)
(AG) (AU) (AG) (AU) (AG) (AG) (AU) (AU) (AG) (AG)
(AU) (AU) (AG)
The electronic state is 1-AG.
Alpha  occ. eigenvalues --  -89.02677 -89.02677 -89.02656 -89.02655 -89.02645
Alpha  occ. eigenvalues --  -89.02644 -89.02637 -89.02637 -16.95161 -16.84975
Alpha  occ. eigenvalues --  -14.40883 -14.40883 -14.40875 -14.40875 -13.09848
Alpha  occ. eigenvalues --  -13.09674 -13.06568 -13.06516 -13.01565 -13.01242
Alpha  occ. eigenvalues --  -10.34201 -10.34171 -10.32389 -10.32389 -10.32355
Alpha  occ. eigenvalues --  -10.32355 -10.27799 -10.27799 -10.27750 -10.27750
Alpha  occ. eigenvalues --   -9.05920  -9.05822  -8.98323  -8.98251  -8.97671
Alpha  occ. eigenvalues --   -8.97624  -8.94969  -8.94934  -8.94582  -8.94398
Alpha  occ. eigenvalues --   -8.09141  -8.09139  -8.09130  -8.09129  -8.09126
Alpha  occ. eigenvalues --   -8.09125  -8.09089  -8.09089  -6.05629  -6.05628
Alpha  occ. eigenvalues --   -6.05617  -6.05616  -6.05534  -6.05534  -6.05498
Alpha  occ. eigenvalues --   -6.05497  -6.04996  -6.04995  -6.04985  -6.04984
Alpha  occ. eigenvalues --   -6.04934  -6.04934  -6.04897  -6.04897  -6.04814
Alpha occ. eigenvalues --   -6.04814  -6.04774  -6.04774  -6.04682  -6.04682
Alpha  occ. eigenvalues --   -6.04670  -6.04669  -2.59063  -2.36105  -1.04745
Alpha  occ. eigenvalues --   -1.04739  -0.97301  -0.97300  -0.96051  -0.91483
Alpha  occ. eigenvalues --   -0.91008  -0.89423  -0.88270  -0.86042  -0.85970
Alpha  occ. eigenvalues --   -0.83941  -0.80777  -0.80523  -0.74075  -0.70454
Alpha  occ. eigenvalues --   -0.70382  -0.70252  -0.69783  -0.66156  -0.63141
Alpha  occ. eigenvalues --   -0.62128  -0.60216  -0.58688  -0.57419  -0.57038
Alpha  occ. eigenvalues --   -0.56630  -0.55494  -0.53278  -0.51991  -0.51965
Alpha  occ. eigenvalues --   -0.50957  -0.48728  -0.48724  -0.48490  -0.47258
Alpha  occ. eigenvalues --   -0.46103  -0.46099  -0.46078  -0.43018  -0.42908
Alpha  occ. eigenvalues --   -0.42638  -0.42094  -0.42006  -0.41231  -0.40676
Alpha  occ. eigenvalues --   -0.40584  -0.40544  -0.39476  -0.38599  -0.37515
Alpha  occ. eigenvalues --   -0.37043  -0.35913  -0.34534  -0.34530  -0.34339
Alpha  occ. eigenvalues --   -0.33407  -0.32686  -0.32370  -0.32148  -0.31927
Alpha  occ. eigenvalues --   -0.31403  -0.28076  -0.27924  -0.21495
Alpha virt. eigenvalues --   -0.18780  -0.17991  -0.16068  -0.15495  -0.14251
Alpha virt. eigenvalues --   -0.12118  -0.09062  -0.09049  -0.08307  -0.07419
```

```
Alpha virt. eigenvalues --   -0.06317  -0.05808  -0.05609  -0.04542  -0.02146
Alpha virt. eigenvalues --   -0.00905  -0.00298  -0.00137   0.01135   0.01395
Alpha virt. eigenvalues --    0.01745   0.01945   0.02252   0.02526   0.02918
Alpha virt. eigenvalues --    0.03003   0.03840   0.03898   0.03985   0.04459
Alpha virt. eigenvalues --    0.05748   0.07954   0.07955   0.11330   0.11556
Alpha virt. eigenvalues --    0.12901   0.14809   0.15070   0.15437   0.15529
Alpha virt. eigenvalues --    0.18848   0.20052   0.21524   0.25338   0.25866
Alpha virt. eigenvalues --    0.27010   0.27198   0.28544   0.28611   0.29713
Alpha virt. eigenvalues --    0.29991   0.30148   0.31204   0.32098   0.32262
Alpha virt. eigenvalues --    0.32593   0.32757   0.32946   0.35747   0.35929
Alpha virt. eigenvalues --    0.36719   0.36920   0.37338   0.37846   0.38287
Alpha virt. eigenvalues --    0.38655   0.41632   0.41736   0.42267   0.42438
Alpha virt. eigenvalues --    0.42478   0.43101   0.43693   0.44506   0.48353
Alpha virt. eigenvalues --    0.48479   0.50734   0.51436   0.51468   0.52529
Alpha virt. eigenvalues --    0.54352   0.54488   0.55476   0.56271   0.57848
Alpha virt. eigenvalues --    0.58472   0.59197   0.59420   0.59509   0.59620
Alpha virt. eigenvalues --    0.60246   0.61400   0.61909   0.62070   0.62676
Alpha virt. eigenvalues --    0.62876   0.63169   0.64158   0.64660   0.64980
Alpha virt. eigenvalues --    0.65554   0.66061   0.69483   0.70178   0.70293
Alpha virt. eigenvalues --    0.74686   0.75977   0.75983   0.77278   0.80549
Alpha virt. eigenvalues --    0.83290   0.83764   0.84224   0.85224   0.85327
Alpha virt. eigenvalues --    0.85329   0.88923   0.88967   0.89075   0.92493
Alpha virt. eigenvalues --    0.92684   0.93963   0.96912   0.97205   0.97297
Alpha virt. eigenvalues --    0.97533   1.03331   1.06936   1.07034   1.11499
Alpha virt. eigenvalues --    1.11563   1.18934   1.19736   1.23403   1.24086
Alpha virt. eigenvalues --    1.29425   1.29482   1.45610   1.45678   1.46217
Alpha virt. eigenvalues --    1.46460   1.82063   1.82085
```

6. Electrolytic absorption measurement.

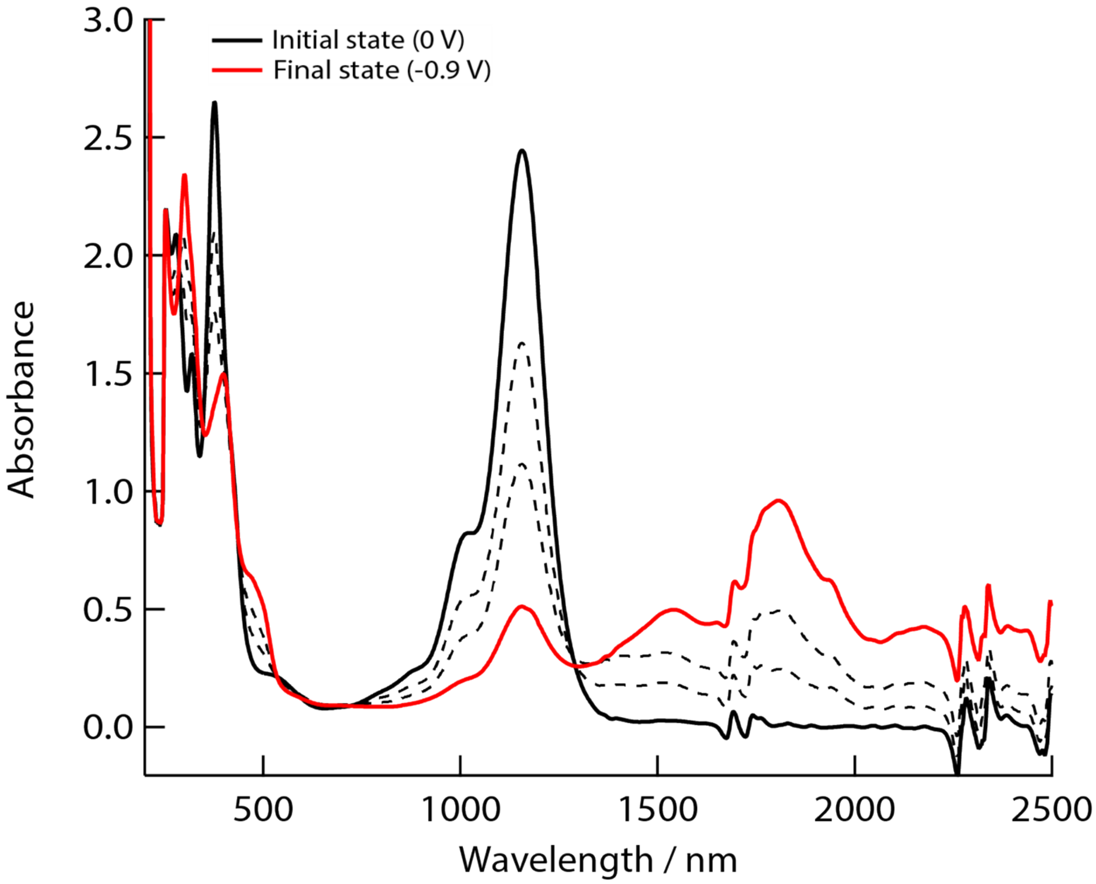

Fig. S6. Electrolytic absorption spectra of complex **1** in 0.1 M ^{n}Bu$_4$NClO$_4$ / DMSO solution under -0.9 V potential (vs. Fc/Fc$^+$) at an ambient temperature. Around 1500 nm, broad peak arose corresponding to some transitions involving one electron reduced state of complex **1** as well as chemically reduced measurement in Fig. 3.

7. Electronic absorption measurement.

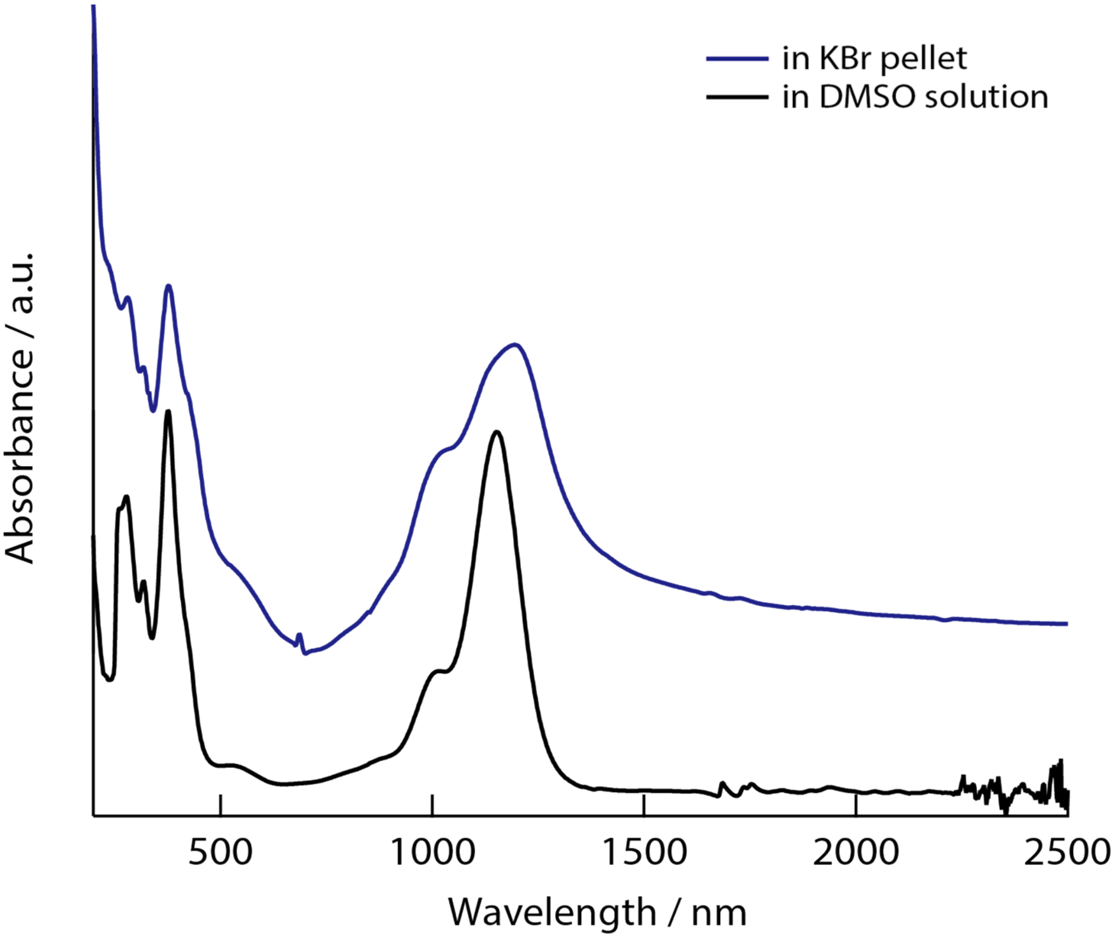

Fig. S7. Electronic absorption spectra of complex **1** in KBr pellet (blue line) and DMSO solution (black line). Most intense peaks around 1150 nm were assigned to the transition from HOMO to LUMO calculated by TD-DFT method.

Table S2. Photochemical data of complex **1**.

Condition	Absorption in NIR region	
	λ / nm	$\varepsilon_{\mathrm{max}}$ / M^{-1} cm^{-1}
KBr pellet	1182, 1004	—
DMSO sol.	1153, 1004	14000, 3300

8. Reference.

(1) Y. Kobayashi, B. Jacobs, M. D. Allendorf, J. R. Long, *Chem. Mater.* **2010**, *22*, 4120-4122.